ANALYSIS OF THE VORTICAL FLOW AROUND A 60 DEGREE DELTA WING WITH VORTEX FLAP

ICAS-86-2.5.5

B. Sung* and J.F. Marchman, III**

Virginia Polytechnic Institute and State University
Blacksburg, Virginia 24061, U.S.A.

Abstract

Subsonic wind tunnel investigation were conducted on a 60 degree swept, flat plate, delta wing with a leading edge vortex flap at a Reynolds number of about 2.14 millions. The optimum flap deflection angles were found where the primary vortex was confined to the leading edge flap. It was also found that the flap deflection could be used to restore a vortex flow from burst vortex condition. A non-linear vortex lattice code with a new velocity jump formula was developed to predict the aerodynamic characteristics of the delta wing. The current method improved over other non-linear vortex lattice methods by predicting the pressure distributions, but the suction peak pressures were lower and the location of the suction peaks were predicted farther from the leading edge than the experimental results.

Nomenclature

A	: Influence coefficient
C	: Wing root chord
$\bar{c}$	: Mean aerodynamic chord
C_D	: Drag coefficient
C_{Di}	: Induced drag coefficient
C_{Do}	: Drag coefficient at zero lift
C_L	: Lift coefficient
C_M	: Pitching moment coefficeint at 1/4 $\bar{c}$
C_p	: Pressure coefficient
G	: Strength of the vortex loop
$\hat{n}$	: Unit normal vector
P	: Static Pressure
P_t	: Total Pressure
q	: Dynamic Pressure
α	: Angle of attack
$\vec{\gamma}$	: Strength of vortex sheet
$\vec{\Gamma}$	: Strength of vortex filament
δ	: Flap deflection angle
μ	: Doublet strength
ρ	: Air density
∞	: Free stream condition

* Research scientist, Korean Institute of Machinery and Metals, Changwon, Korea

** Associate Professor

Copyright © 1986 by ICAS and AIAA. All rights reserved.

Introduction

The leading edge (L.E.) vortex flap has received considerable attention recently as a device to improve the aerodynamic performance of highly swept delta wings (1-6). Most researchers to date have concentrated on the overall aerodynamic performance characteristics of the flaps such as forces and moments. In order to truly optimize the use of the vortex flap, more research is needed on the details of the flow over the delta wing-flap system and local pressure distributions on delta wing with a vortex flap.

There has apparently been a problem in applying existing computational programs to a 60° sweep delta wings or a vortex flapped 60° sweep delta wing. Most literature to date has not computed the case of a 60° delta wing and some researchers (7, 8) reported that they could not obtained a converged solution or had difficulty in obtaining a solution. Free Vortex Sheet (FVS) code (9, 10) developed by Boeing Company and similar code (11) developed by NLR of the Netherlands are the only currently availabe computational programs for predicting the pressure distributions on a delta wing. But it is still "expensive" to use such codes during the preliminary design phase of the aircraft where number of configurations are studied. For example Erickson (12) reported that FVS code took 500-1300 CPU seconds on the Cyber 175 computer to yield a converged solution for a flapped delta wing case using the converged solution of a similar case as a starting guess; therefore it would take more CPU time to run for different design cases.

Therefore the purpose of the current study is to analyze the phenomena associated with a 60° delta wing with vortex flap, investigate the possibility of delaying the vortex breakdown using a vortex flap, and study the optimum angles of flap deflection at various angles of attack. Also, the present work attempts to develope an "inexpensive" computational code to predict the pressure distribution which can be used in the preliminary design phase of the aircraft.

Experimental Procedure

The experimental study was conducted in the 6 ft x 6 ft, straight test section of the Virginia Tech. Stability Wind Tunnel using a flat plate, half span, 60° sweep back delta wing with constant chord L.E. flap and a 1.27 m root chord. The details of the delta wing model are shown on Fig. 1. The flap chord to wing root chord ratio was 0.095, which was based on the earlier tests by Marchman (1).

In order to provide a smooth wing surface, 1.6 mm O.D. copper tubings were inlaid into grooves on the wing surface, and 47 pressure tabs of 0.5 mm were drilled along 4 lines perpendicular to the L.E. of the wing after final finishing of the wing surface. All the pressure tubes connected to the pressure tabs were buried inside the delta wing and connected to the pressure scanner which was located immediately outside the test section to reduce the time lag inherent in any pressure measuring system which may be caused by long leads from the pressure ports to the pressure transducer. The maximum projected area of the model to the wind tunnel test section plane normal to the free stream was 12.5 % when the angle of attack was 40° with zero flap deflection.

The half span delta wing model was mounted vertically on the turntable installed on the test section floor and the angle of attack were set by rotating the turntable with accuracy of 0.1°. The flap deflection angle was adjusted with the error less than 0.3°. Throughout the tests, 25 readings were taken and averaged for each datum. The pressure distribution investigations were performed at a Reynolds number of about 2.14 millions based on the root chord of the delta wing, through a range of angle of attack from zero to 40° with flap deflection angle from zero to 45°, both in 5° increments. Tuft flow visualization tests were conducted in an attempt to correlate the flow pattern and pressure distributions, and to investigate the behavior of the vortex flow above the wing surface. The mean flow field surveys were performed for angles of attack of 10° and 15° with flap deflection angle of 10° and 30°. For each case, the flow fields were measured at 3 different planes over the wing surface which were perpendicular to the free stream and located at x/C=0.375, 0.625 and 0.875 each. During the mean flow field survey, a 5-hole yawhead probe was used to measure the flow properties such as flow velocity components, total pressure, and static pressure distributions. To avoid the vibration of the yawhead probe support, the mean flow field measurements were done at the reduced free stream velocity and the Reynolds number was about 1.50 millions based on the root chord of the delta wing. The yawhead probe was also calibrated at the same free stream velocity as the mean flow field measurement, which resulted the Reynolds number of 3780 based on the probe tip diameter.

Experimental Results

It was found that the flap deflection angle plays a decisive role in determining the flow pattern around a delta wing with flap, as expected. For each flap deflection angle, there is a range of angle of attack which has distinct flow characteristics. Generally, the vortex flow started on the L.E. of the flap at small angle of attack and only a small portion of the flap was affected by the vortex flow. With increasing angle of attack, the area affected by the vortex flow was increased. When the angle of attack at which a given flap angle was optimum was exceeded, the vortex core moved inboard of the wing and then started to burst at the rear part of the wing. The vortex bursting point moved from the trailing edge to the apex with increasing angle of attack. A map of the flow regime (Fig. 2) corresponding to above mentioned phenomena on a delta wing with flap, was made from the results of the experiments. The optimum flap deflection angle, δ_{opt}, was defined as the flap deflection angle where the reattachment line at x/C=0.75 was placed on the flap hinge line at each angle of attack. At $\delta=\delta_{opt}$, most of the primary vortex was above the flap, in other words, the primary vortex was confined to the L.E. flap, thus producing a thrust on the flap surface and increasing the lift/drag ratio due to the low pressure caused by the vortex flow.

The surface streamlines were sketched based on the flow visualization experiments using woolen tuft. Typical cases of pressure distibutions and corresponding sketches of the surface streamlines are shown on Fig. 3 and 4. Comparing the streamlines with the pressure distributions, one can see that the pressure distributions coinside exactly with the surface streamline patterns in such details as the primary vortex reattachment line and the secondary separation line.

The pressure distribution results showing the effects of the flap deflection at different angle of attack are shown on Fig. 5 - 8. Pressure distributions are plotted on a rotated axis where X' represents the distance along the flap hinge line from the wing apex, and Y' corresponds to the distance from the flap hinge line. Therefore, $Y'>0$ on the flap surface and $Y'<0$ on the wing surface, i.e. inboard of the flap hinge line. The effect of the flap deflection on a pressure distribution started to appear at $\alpha=5^\circ$, although it is still a weak vortex flow. The flap deflection effect become evident from $\alpha=10^\circ$ (Fig. 5), since the vortex was well developed at $\alpha=10^\circ$ with $\delta=0^\circ$. Generally, increasing the flap deflection at a fixed angle of attack reduce the strength of the vortex flow and the vortex core moved to the L.E. of the flap.

At $\alpha=15^\circ$ (Fig. 6), small flap deflection ($\delta<15^\circ$) weakened the vortex flow so the negative pressure peaks are reduced, which is similar to the case of $\alpha=10^\circ$. But at moderate flap deflection ($15^\circ\leq\delta<30^\circ$), not only did the negative pressure peaks move outward from the wing centerline, but also the negative pressure peaks are increased. The small flap deflection weakened the strength of the primary vortex and the primary vortex remains in merged vortex flow with the separated flow from the apex edge. With moderate flap deflection, the separated bubble on the apex detached from the primary vortex which resulted in a weaker and smoother negative pressure distribution near the apex. The weak primary vortex generated a weak adverse pressure gradient below the vortex core, therefore the secondary vortex region was reduced. As the seceodary vortex region was reduced, the primary vortex core moved closer to the L.E. (downward and outboard shift), and this shift of the vortex core induced a higher velocity on the flap surface resulting in a strong negative pressure peak near the leading edge. A large flap deflection ($\delta\geq30^\circ$) weakened the primary vortex so much that the secondary vortex disappeared and the negative pressure peak decreased as flap deflection increased above a moderate flap angle.

Another benefit of the flap deflection shown in Fig. 6 is the restoration of the vortex flow where bursting had occured at lower flap deflection.

The primary vortex flow is restroed at α=15° with a flap deflection δ>20° at X'=1.011, where the primary vortex had burst with δ=0°. The restoration of the vortex flow is due to the decreased adverse pressure gradient along the vortex core with flap deflection. The restoration of the vortex flow (or suppression of the vortex bursting) is clear at α=20° (Fig. 7), where the flap deflection of $\delta \geq 25°$ restored the vortex bursting at X'=0.722. The shift of the vortex core and increased suction peak are also seen at α=20°(Fig. 7). The burst vortex near the trailing edge can not be suppresed at α=20°. At high angle of attack where the vortex burst from the apex, flap deflection can restore the vortex flow only in near the apex. One can see that the vortex is restored only up to X'=0.433 at α=30°, by a flap deflection of δ=45° (Fig.8). At α=35°, it was not possible to suppress the vortex bursting from the apex. Further increasing the angle of attack up to α=40°, the flow was completely stalled, therefore the flap was ineffective as a means of aerodynamic performance improvement.

It might be possible to restore the vortex flow near the apex at high angles of attack by large flap deflection, but deflecting the L.E. flap more than 45° does not appeared to be a practical way to improve aerodynamic performance, when one compares the gain in lift in light of the structural requirement of the flap and increased drag. If one assume that the operating range of the delta wing is determined by the criteria of the presence of a well established voretex flow up to 50 % of the wing chord, then the operating range of this type delta wing will be α=5° - 30°.

A typical velocity vector plots, the static pressure contour plots and the total presssure contour plots are made from the mean flow field measurement and are shown in Fig. 9 - 11. In Fig. 9 - 11, the flow properties were plotted on the plane perpendicular to the free stream. Z and W represent the axis perpendicular to the free stream and Y-axis, and the velocity in Z direction, respectively. The vortex sheet location was determined by tracing the local maximum of the velocity which is plotted as dashed line. The cross sectional shapes of the vortex sheet are elliptical for the 60° delta wing rather than the circular shape usually found on higher sweep delta wings. This might be the reason of having difficulty to get the converged solution for 60° delta wing using other computational computational. The general shape of the static pressure contour is sprial compared to the concentric ellipse for the total pressure contour.

The velocity vector plots in the Y-Z plane for the case of α=15° with δ=10° are shown in Fig. 9, and the corresponding static pressure and total pressure isobars are shown in Fig. 10 and 11, respectively. The effect of the secondary vortex on the velocity vector plot was so small that it can only be recognized from the slight upward inclination of the velocity vector, since the secondary vortex is a separation bubble inside the boundary layer. The secondary vortex can be seen clearly in total pressure plot, where the region containing the secondary vortex is shown by the closed region of reduced total pressure. The effect of the vortex bursting is also shown in Fig. 9 - 11, where the vortex burst at X=0.75. The effects are the enlarged shape of the vortex sheet, and reduced gradient of the tangential velocity, static pressure, and total pressure in the radial direction at the station downstream of the bursting point. Also the region of minimum total pressure and minimum static pressure are widened after vortex bursting. All the above phenomena were caused by the resulting turbulent mixing process inside of the burst vortex flow.

Computational Approach

A non-linear vortex lattice code was developed to predict the pressure distributions on the wing surface. For a flow over a wing at a high Reynolds number, the viscosity effects are limited to the boundary layer on the surface. The vorticity is created in the boundary layer and the votices are formed along sharp edges. Therefore, the flow over a thin wing can be modelled as a potential flow with vortex sheets representing the wing and wake. In current study, the wing surface was divided into a finite number of surface panels. Each surface panel was made up of straight vortex filaments fixed at the edge of the panel, forming a closed vortex loop with constant circulation. Free vortex sheets were represented by free vortex filaments starting from the edge of the wing and extending to infinity. Each free vortex filament consisted of a series of short straight segments and one final semi-infinite segment. To satisfy the Kutta condition, no vortex filaments were placed along the edge of the wing, but vortex filaments were placed perpendicular to the edge of the wing. The panels on the edge of the wing formed closed vortex loops by including the vortex filaments at infinity which were starting vortices. The control points were located at the geometric centers of the surface filaments. The panel arrangement including the initial guess for the free vortex filaments is shown in Fig. 12. The solid lines represent the vortex loop panels and dashed lines refer the free vortex filaments. The edge of the wing is represented by a dotted line and the control points are denoted by (+) symbols. By using the vortex loop panels the number of the unknowns are reduced and the influence coefficient matrix becomes diagonally dominant.

For current study, the vortex loop panel was not shifted one quarter of the local panel chord, while most other researchers (13-17) put the vortex filaments shifted back one quarter-chord length from the edge of the panel (c/4 rule) where c refers to the local panel chord. Since the c/4 rule was developed for the two-dimensional lifting problem to provide a good estimation on the pitching moment coefficient, there was no obvious reason to use this rule for the three-dimensional problems like delta wings.

The Biot-Savart law was used to calculate the induced velocity due to the segments of vortex filaments. Using the vortex loop panels, the governing equation for a M paneled wing can be written as,

$$[A]\{G\} = \{R\} \qquad (1)$$

where

$$[A] = \begin{bmatrix} A_{11} & A_{12} & \cdots & A_{1M} \\ A_{21} & A_{22} & \cdots & A_{2M} \\ \cdot & \cdot & \cdots & \cdot \\ \cdot & \cdot & \cdots & \cdot \\ \cdot & \cdot & \cdots A_{ij} \cdots & \cdot \\ \cdot & \cdot & \cdots & \cdot \\ \cdot & \cdot & \cdots & \cdot \\ A_{M1} & A_{M2} & \cdots & A_{MM} \end{bmatrix}$$

$$\{G\} = (G_1, G_2, \ldots G_j \ldots\ldots G_M)^T$$

$$\{R\} = (R_1, R_2, \ldots R_i \ldots\ldots R_M)^T$$

A_{ij} is the normal component of the induced velocity at the i-th control point by a vortex loop with unit strength at the j-th panel, G_j is the strength of the vortex loop at the j-th panel. and $R_i = -V_{ni}$ is the normal component of the free stream velocity at the i-th control point. G was taken positive for the clockwise vortex loop which induced a velocity in the negative Z direction in Fig. 12.

The boundary conditions for the current problem are;

1. Flow must be tangential to the wing surface.
2. The Kutta condition should be satisfied at the leading edge and trailing edge of the wing.
3. Free vortex sheets are force-free.
4. Spatial conservation of the vorticity should be enforced at the vortex sheet.

The first boundary condition was used to construct the governing algebraic equation (1) for the strength of the vortex loop. The vortex filaments were not placed on the leading and trailing edge of the wing except the apex edge to satisfy the second boundary condition. The third boundary condition was used to relax the position of the free vortices to a force-free position after the strengths of the vortex loops were obtained. The fourth boundary condition satisfied automatically by adopting the vortex loop panels, otherwise additional equations are needed at each corner of the vortex loop panels.

This is a non-linear problem because the strength of the vortex loops and the location of the free vortex are unknown and the strength of the vortex loops are the function of the location of the free vortices, and vice versa. Thus the governing equation (1) can be written,

$$[A(G)]\{G\} = \{R\} \qquad (2)$$

The equation can be solved by an iterratively,

$$\{G^{k+1}\} = [A(G^k)]^{-1}\{R\} \qquad (3)$$

Initial guesses for the positions of the free vortices were needed at the beginning, since the vortex filament positions are the part of the solution.

Every iteration step consists of calculating $[A(G^k)]$, solving $\{G^{k+1}\}$ by using the Gauss-Seidel iterative method, and relaxing the free vortices to the force-free position. This procedure was repeated until both {G} and the positions of the free vortices converged within the pre-set convergence criteria. The aerodynamic loads were computed after the convergences were achieved for both positions of the free vortices and the strength of the vortex loop {G}.

During the relaxation of free vortices to the force-free position, a constant characteristic time step was used rather than a contant vortex segment length. The j+1 th sement of the i-th free vortex can be expressed as,

$$\vec{r}_{i\,j+1} = \vec{r}_{ij} + \vec{V}(\vec{r}_{ij})\Delta t_c \qquad (4)$$

where $\vec{V}(\vec{r}_{ij}) = \vec{V}_\infty + \vec{V}_i(\vec{r}_{ij})$

$\vec{r}_{ij}$: position of the nodal point

$\vec{V}_i(\vec{r}_{ij})$: induced velocity at $\vec{r}_{ij}$

Δt_c : characteristic time step

One unit of the characteristic time step corresponds to the required time to pass the delta wing from the apex to the trailing edge with free stream velocity.

The convergence of the free vortex position was checked by,

$$\max\left[\frac{|r_{ij}^{k+1} - r_{ij}^{k}|}{V_\infty \Delta t_c}\right] \le \varepsilon_F \qquad (5)$$

where ε_F is the convergence tolerance for the free vortices

Aerodynamic Load Caculation

The velocity jump across the vortex sheet is,

$$\Delta\vec{V} = \vec{\gamma} \times \hat{n} \qquad (6)$$

The velocity discontinuity can not be obtained at the control point in a strict sense because the wing was modeled with vortex loop panels. The purpose of this computational program was not to find an exact solution, but an approximate solution was desired. Therefore the same order of approximation was required to obtain the velocity jump as the wing was modeled. To obtain a velocity jump, the vortex loop panel was considered as a constant doublet strength panel since both panels produce the same induced velocity. A surface doublet distribution of density μ can be replaced by an equivelent surface vortex distribution (18) where the vortex sheet strength $\vec{\gamma}$ at each surface surface points satisfies the relation,

$$\vec{\gamma} = -\hat{n} \times \nabla\mu \qquad (7)$$

A doublet panel with constant positive strength μ induces the same velocity field at every field points as a counter-clockwise vortex loop with strength μ, provided that the edges of the panel coincide with the vortex loop. Referring to Fig. 13, the mean slope of the doublet panel at the i-th panel is

$$-\mu_x = \frac{G_{i+1} - G_i}{2l_x} \qquad (8.a)$$

$$\mu_i = \frac{G_{i+n} - G_{i-n}}{2l_y} \qquad (8.b)$$

A mean vortex strength can be obtained using equation (7) and (8), that is,

$$\vec{\gamma} = -\Sigma\Gamma_i\vec{l}_i/(2A) \qquad (9)$$

$i=1,2,3,4$

choosing $\Gamma_1=G_{i+n}$, $\Gamma_2=G_{i+1}$, $\Gamma_3=G_{i-n}$, $\Gamma_4=G_{i-1}$,

$\vec{l}_1=l_x\hat{i}$, $\vec{l}_2=-l_y\hat{j}$, $\vec{l}_3=-l_x\hat{i}$, $\vec{l}_4=l_y\hat{j}$,

and $A=l_x l_y$,

Above formula can be extended to any polygonal panel. The velocity jump can be calculated using equation (6) after the mean vortex strength is obtained.

After the velocity jump is obtained, the pressure can be found by using Bernoulli's equation. The total pressure was assumed to be constant near the wing surface. Since only steady cases were considered,

$$P + \tfrac{1}{2}\rho V^2 = P_\infty + \tfrac{1}{2}\rho V_\infty^2 \qquad (10)$$

The velocities on the upper surface and lower surface at the control points are,

$$\vec{V}_u = \vec{V}_\infty + \vec{V}_i + \tfrac{1}{2}\Delta\vec{V}$$
$$\vec{V}_l = \vec{V}_\infty + \vec{V}_i - \tfrac{1}{2}\Delta\vec{V} \qquad (11)$$

The pressure coefficients for both surfaces become,

$$C_{pu} = 1 - (V_u/V_\infty)^2$$
$$C_{pl} = 1 - (V_l/V_\infty)^2 \qquad (12)$$

The normal force coefficient and axial force coefficient are obtained by summing up the pressure differences multiplied by each panel area. The pitching moment was calculated for a half chord point of the root chord which is the 1/4 chord point from the leading edge of the mean aerodynamic chord.

$$C_N = \Sigma(C_{pl} - C_{pu})_i n_z A_i/A$$
$$C_A = \Sigma(C_{pl} - C_{pu})_i n_x A_i/A \qquad (13)$$
$$C_M = [\Sigma(C_{pl} - C_{pu})_i\{n_z(x_{ac} - x) + n_x z\}A_i]/A\bar{c}$$

$i=1,2, \ldots\ldots\ldots, M$

where A_i : area of the i-th panel

A : total area of the wing projected on the x-y plane

x, z: coordinate of the i-th control point

n_x, n_z: x and z component of the i-th unit normal vector

Then the lift coefficient and drag coefficient are,

$$C_L = C_N\cos\alpha - C_A\sin\alpha \qquad (14)$$
$$C_{Di} = C_N\sin\alpha + C_A\cos\alpha$$

Computational Result and Discussion

Prior to running the computational program for various cases, the effects of the certain parameters on the computational results were tested, and proper values were selected for each parameter based on the quality of the result, numerical stability, and required execution time to get the converged result. The main wing was divided into NW x (NW + 1)/2 panels, and NW x NF panels were used to represent the flap where NW refers to the number of vortex loop panel rows on a wing and NF is the number of vortex loop panel columns on a flap.

The first parameter considered was the number of the panels. The cases tested were NW x NF = 6x2, 7x3, and 9x4; the total number of panels are 33, 49, and 81 respectively. The general shapes of the pressure distribution were the same but the suction pressure increased in small amount with an increase in the number of panels, and the resulting aerodynamic loads were also increased slightly. The effect of the number of the vortex loop panel columns on the flap (NF) were also tested, and found that it does not affect the flow around a delta wing significantly. The shape of the converged free vortices were unchanged for different value of NF.

The characteristic time step Δt_c has considerable influence on the pressure distributions and the shape of the free vortices. Compared to the larger time step, using a small time step yielded a better result closer to the experimental result as it rendered a tighter rolled-up leading edge vortex thus resulting in a suction peak placed closer to the leading edge of the flap. But it required more CPU time to relax a single vortex filament and also more iteration steps to result in a converged shape of the free vortices, and sometimes free vortices were not converged into the force-free positions. Therfore, one needs a compromise between the quality of the result, CPU time and the risk of non-convergence. After considering several cases, Δt_c=0.07 was chosen for the current study. The first shedding distance (FEDG) of the free vortices from the leading edge has a more significant effect than the characteristic time step. A shorter shedding distance would simulate the vortex flow closer to the real flow, but sometimes the free vortices tended to penentrate the wing or flap surface during the relaxation and this resulted in a numerical instability of the program and also required more iteration steps for convergence. Therefore, one needs another compromise between the quality of the result and the stability of the numerical procedure. After testing several cases, FEDG=0.03 was chosen which is approximately 32 % of the flap chord.

Generally, the current computational program predicted the suction peak located farther from the leading edge, a lower suction peak pressure and higher C_L than the experimental result. A smaller Δt_c resulted in a suction peak closer to the leading edge, and a smaller value of FEDG gives a lower C_L and higher suction peak pressure which is closer to the experimental result. Hence a certain value of FEDG and Δt_c other than infinitely small value will result an inevitable error in the computational result and it can be reduced by using smaller value.

The cases for the 60° delta wing with leading edge vortex flap were computed using the parameters determined previously and compared with the experimental result. The pressure distributions were computed at the same stations where the pressure tabs were located in experiment. The flap deflection angle used in computation is the same as that in experiment; a surface deflection angle and not a mean camber line deflection angle.

The pressure distribution plots (Fig. 14, and 15) clearly showed the effect of the flap deflection. The suction peak was reduced gradually as the flap deflection angle was increased. The major effects of the flap deflection are reduction in suction peak and shift of the suction peak closer to the leading edge with increase in flap deflection angle. It was impossible to get a converged solution at low angles of attack with larger flap deflection angle because the flow over the flap surface is an attached flow and experiences a positive pressure, hence the vortex filament always tended to penetrate the wing. A typical converged shape of the free vortex filaments is shown on Fig. 16. One interesting phenomenon was that the first free vortex filament shed from the flap apex behaved like a vortex core when the vortex flow was well developed. With increase in flap deflection, the coiled free vortex filaments started to unwind because the vortex strength was decreased and the pressure distributions become flatter. With large flap deflection angle and small angle of attack, which correspond to the vortex starting angle of attack in experiment (Fig. 2), free vortex filaments were placed parallel to the free stream. In that case, the vortex strength was so small that velocity induced by the vortex was much less than the free stream velocity. The location of the suction peak pressure did not shift toward the leading edge because of the uncoiling of the free vortex filaments.

In actual flow the leading edge free vortex sheet is rolled up tightly due to the negative radial pressure gradient, while in computation there was no mechanism to roll up the vortex filaments tightly. This effect combined with the finite length of the vortex segments resulted in a loosely rolled-up leading edge vortex filament and a smaller suction peak near the leading edge.

The current computational method was compared with two other methods (9, 10, 15) for the 74 plain delta wing cases to verify the pressure formula, equation (6). The results for the longitudinal aerodynamic loads are compared in Fig. 17 for angles of attack up to 40 . The current method predicts the total aerodynamic loads quite accurately up to stall angle. Mehrotra's method predicts the lift coefficient and pitching moment quite close to the experimental result. The FVS code predicts the lift coefficient very close to the experimental result while pitching moment and induced drag predictions were not as good as the current method. The pressure distributions were also compared but not included in this paper. A typical execution time was approximately 70 seconds in 12 iterations using the current method on the IBM 3084, while Mehrotra's method took 4540 seconds in 10 iteration on the Cyber 175 (16). The computational speeds of IBM 3084 and Cyber 175 are comparable.

Conclusion

An experimental study was undertaken to investigate the details of the flow phenomena over a delta wing with L.E. vortex flap. Also a non-linear vortex lattice method was developed as a cost-effective prediction tool for the plain or vortex flapped delta wing aerodynamics.

Following are the conclusions drawn from the current research.

Form the experimental study,

1. The L.E. vortex flap was found to be an effective means to control the L.E. vortex flow over a delta wing.
2. The optimum flap deflection angles were found for angles of attack at which most of the L.E. vortex could be confined on the flap.
3. The flap deflection reduces the strength of the L.E. vortex over a delta wing thus reducing the suction peak and shifting suction peak location closer to the L.E.
4. It was possible to restore vortex flow from a burst vortex flow with proper deflection.

From the computational study,

1. The total aerodynamic loads obtained by integration of the pressure distributions over the wing matched well with the experimental result.
2. The first shedding distance of the free vortex filaments has the strongest effects on the converged solutions.
3. The current method under-predicts the suction peak and predict the location of the suction peak farther from the L.E. than the experiment.
4. The current method improved over other non-linear vortex lattice methods by predicting the actual pressures.

References

1. Marchman, J.F., "Effectiveness of Leading-Edge Vortex Flaps on 60 and 75 Degree Delta Wings", J. Aircraft, Vol.18, No.4, 1981, pp.280-286.
2. Lamar, J.E. and Campbell, J.F., "Vortex flaps-advanced control devices for supercruise fighters", Aerospace America, Jan. 1984, pp.95-99.
3. Quinto, P.F. and Paulson, J.W., "Flap Effectiveness on Subsonic Longitudinal Aerodynamic Characteristics of a Modified Arrow Wing", NASA TM 84582, 1983.
4. Frink, N.T., Huffman, J.K., and Johnson, T.D., "Vortex Flap Flow Reattachment Line and Subsonic Longitudinal Aerodynamic Data on 50° to 74° Delta Wings on Common Fuselage", NASA TM 84618, 1983.
5. Rao, D.M., "Vortical Flow Management for Improved Configuration Aerodynamics-recent Experiences", Aerodynamics of Vortical Type Flows in Three Dimensions, AGARD CP 342, 1983.
6. Erickson, G.E. and McCann, M.K., "Experimental and Analytical Investigation of the Subsonic Aerodynamics of Slender Wings with Leading-Edge Vortex Flaps", AIAA paper 83-2113, 1983.
7. Kuhlman, J.M., "Analytical Studies of Separated Vortex Flow on Highly Swept Wings", NASA CR 3022, 1978.

8. Chaturvedi, S.K. and Ghaffari, F., "Study of Highly Sweptback Wings by the Free Vortex Sheet Method", NASA CR 169559, 1982.
9. Weber, J.A., Brune, G.W., Johnson, F.T., Lu, P., and Rubbert, P.E., "The Three Dimensional Solution of Flows over Wings with Leading-Edge Vortex Separation", AIAA J., Vol.14, No.4, April 1976, pp.519-525.
10. Johnson, F.T., Lu, P., Ticono, E.N.,and Epton, M.A., "An Improved Panel Method for the Solution of Three-Dimensional Leading-Edge Vortex Flows; Vol.1-Theory Document", NASA CR 3278, July 1980.
11. Hoejimakers, H.W.M. and Bennekers, B., "A Computational Model for the Calculation of the Flow about Wings with Leading-Edge Vortices", High Angle of Attack Aerodynamics, AGARD CP 247, 1979.
12. Erickson, G.E., "Application of Free Vortex Sheet Theory to Slender Wings with Leading-Edge Vortex Flaps", AIAA Paper 83-1813, 1983
13. Mook, D.T. and Maddox, S.A., "Extension of a Vortex-Lattice Method to include the Effects of Leading-Edge Separation", J. Aircraft, Vol.11, No.2, Feb. 1974, pp.127-128.
14. Kandil, O.A. and Balakrishnan, L., "Recent Improvements in the Prediction of the Leading and Trailing Edge Vortex Cores of Delta Wings", AIAA Paper 81-1263, 1981.
15. Mehrotra, S.C. and Lan, C.E., "A Theoretical Investigation of the Aerodynamics of Low-Aspect-Ratio Wings with Partial Leading-Edge Separation", NASA CR 145304, Jan. 1978.
16. Pao, J.L., and Lan, E.C., "A Vortex-Filaments and Core Model for Wings with Edge Vortex Separation", NASA CR 165847, Feb. 1982.
17. Konstadinopoulous, P., Thrasher, D.F., Mook, D.T., Nayfeh, A.H., and Watson, L., "A Vortex Lattice Method for General Unsteady Aerodynamics", J. Aircraft, Vol.22, No.1, Jan. 1985, pp.43-49.
18. Hess, J.L., "Calculation of Potential Flow about Arbitrary Three-Dimensional Lifting Bodies", MDC J5679-01, Oct. 1972, McDonnell Douglas.

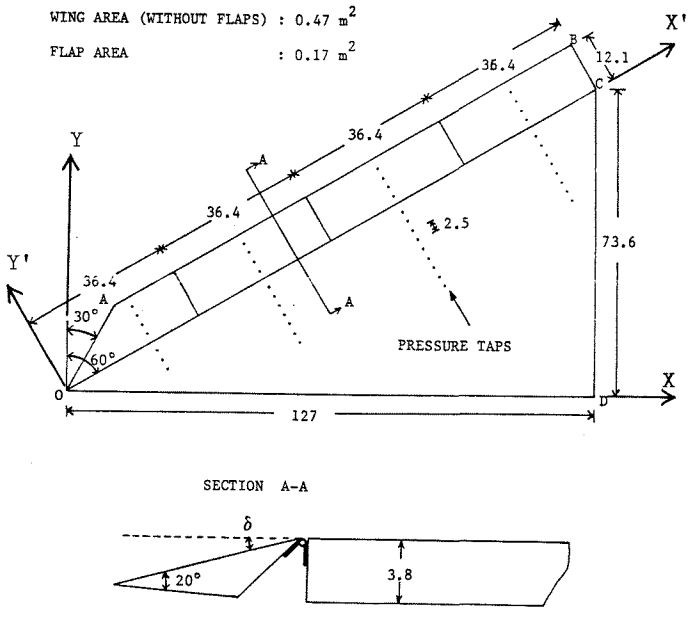

Fig. 1. Geometry of the 60° delta wing model with leading edge vortex flap. Dimensions in centimeters.

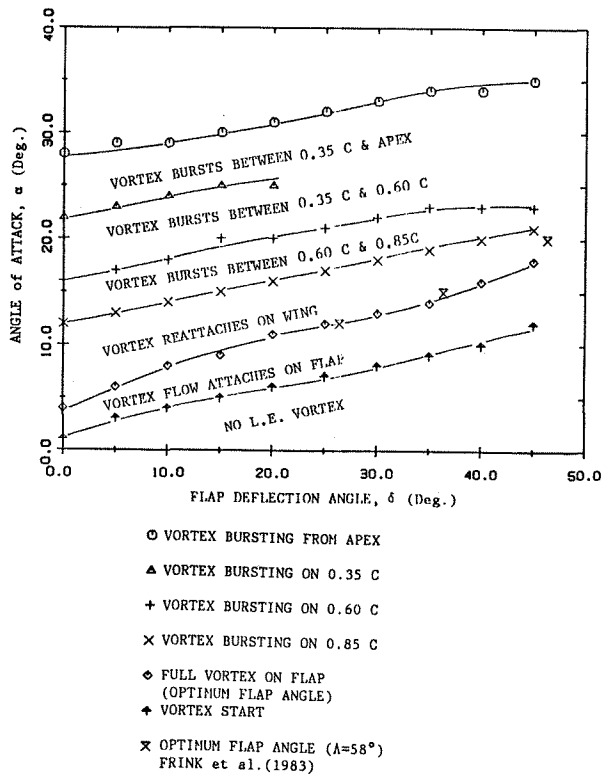

Fig. 2. Flow regime over a 60° delta wing with leading edge vortex flap.

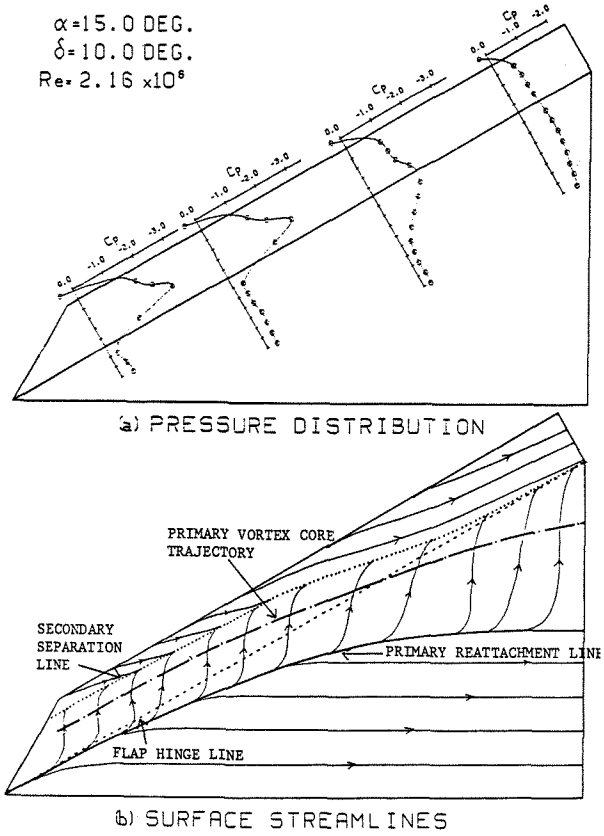

Fig. 3. Pressure distributions and surface streamlines at $\alpha=15°$, $\delta=10°$

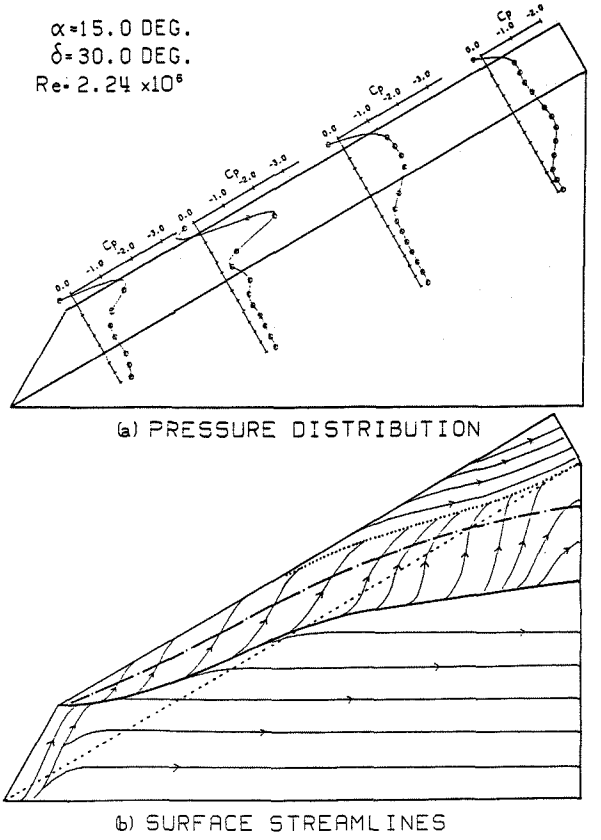

Fig. 4. Pressure distributions and surface streamlines at $\alpha=15°$, $\delta=30°$

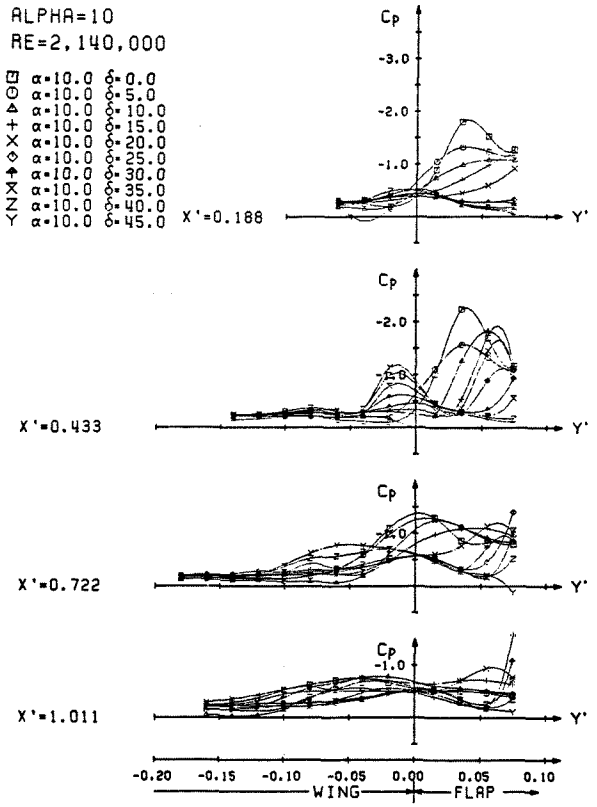

Fig. 5. Effect of flap deflection at $\alpha=10°$ (experiment).

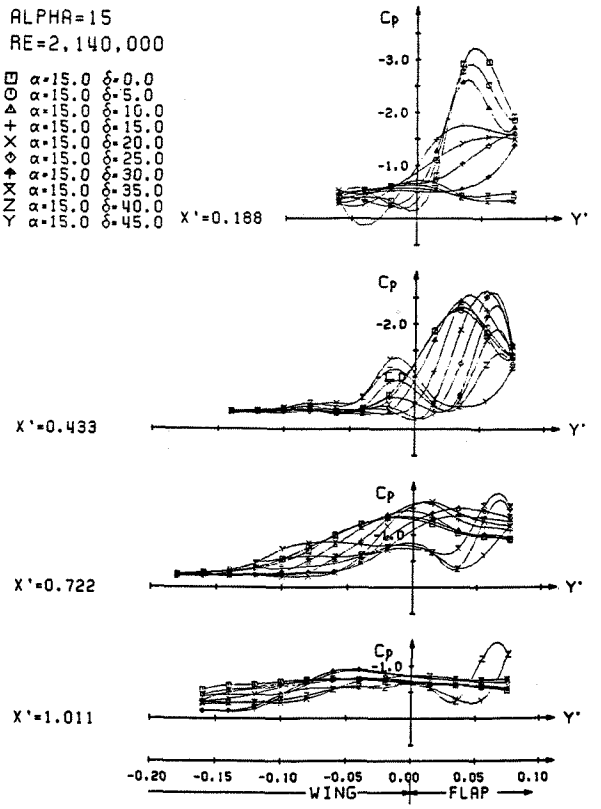

Fig. 6. Effect of flap deflection at $\alpha=15°$ (experiment).

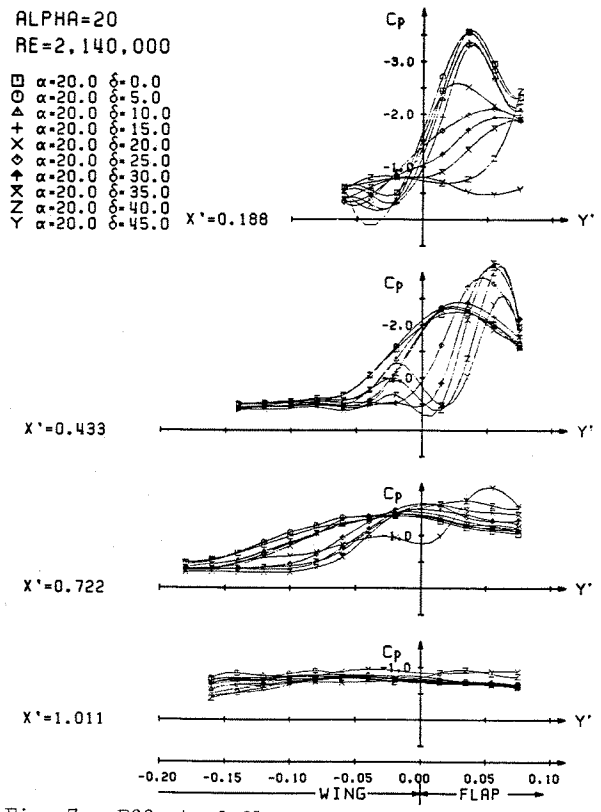

Fig. 7. Effect of flap deflection at $\alpha=20°$ (experiment).

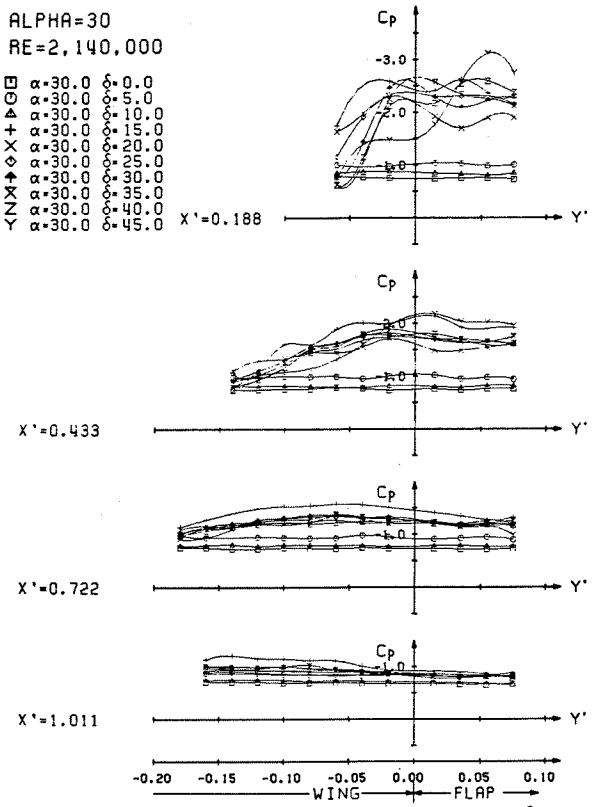

Fig. 8. Effect of flap deflection at $\alpha=30°$ (experiment).

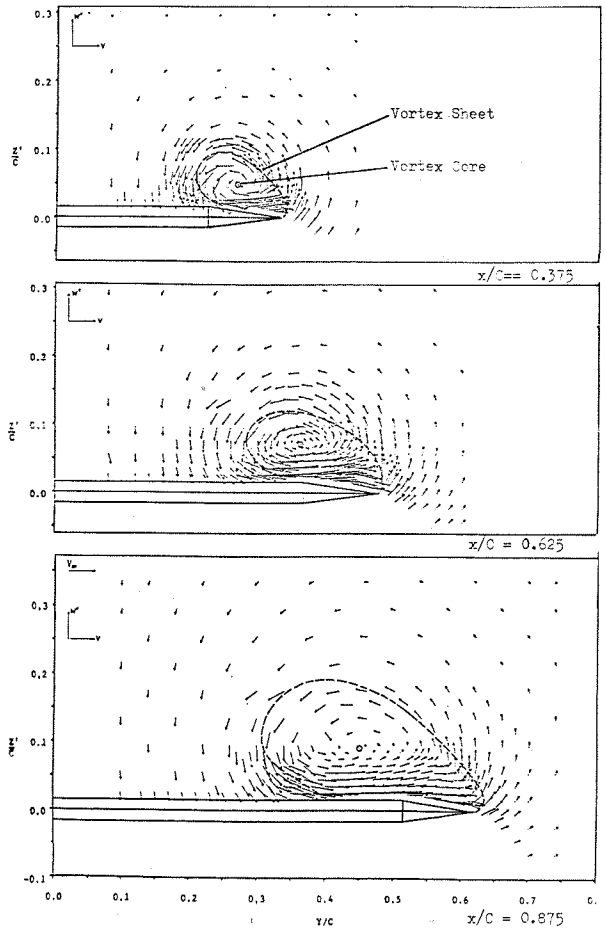

Fig. 9. Velocity vector plot at $\alpha=15°$ with $\delta=10°$

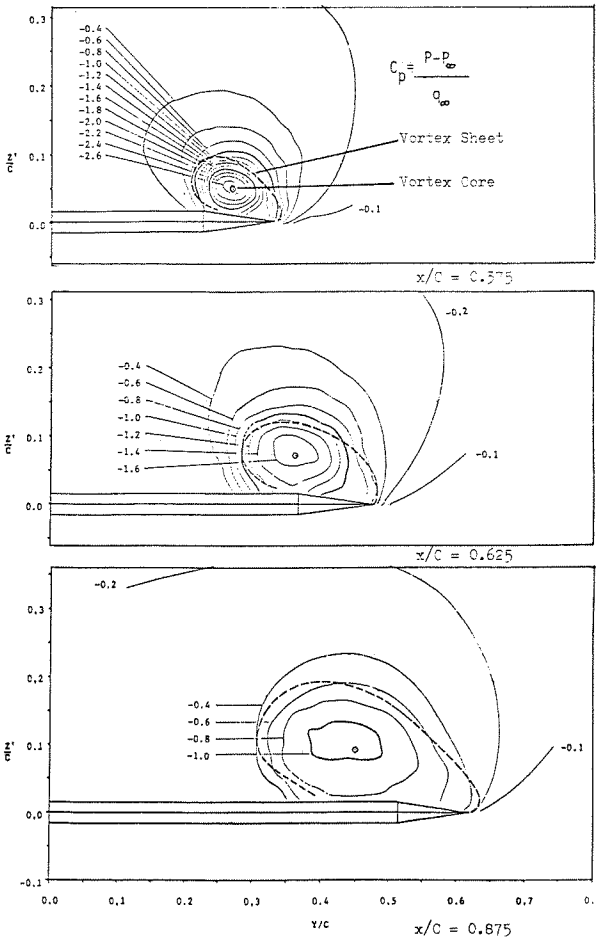

Fig. 10. Static pressure distributions at $\alpha=15°$, $\delta=10°$

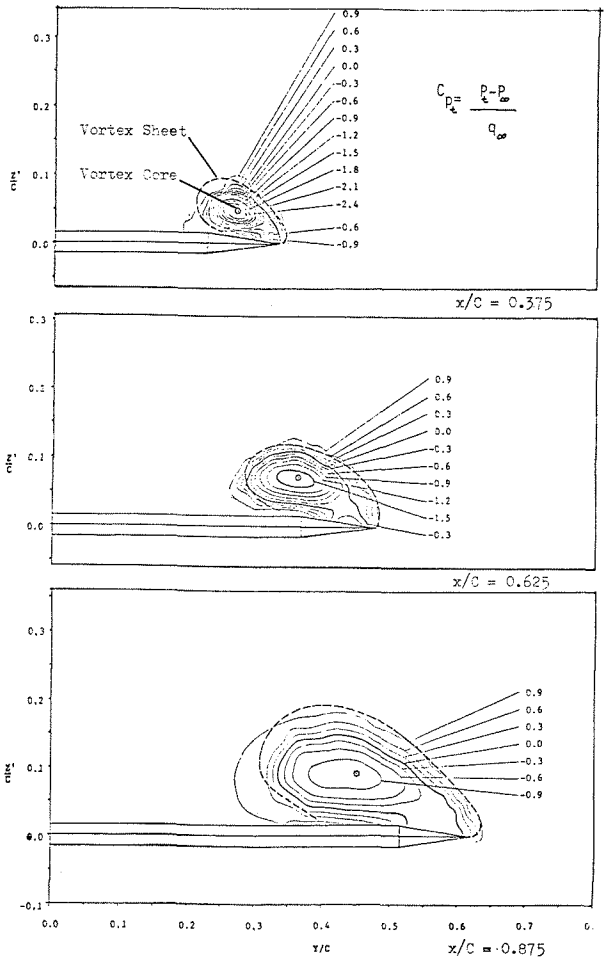

Fig. 11. Total pressure distributions at $\alpha=15°, \delta=10°$

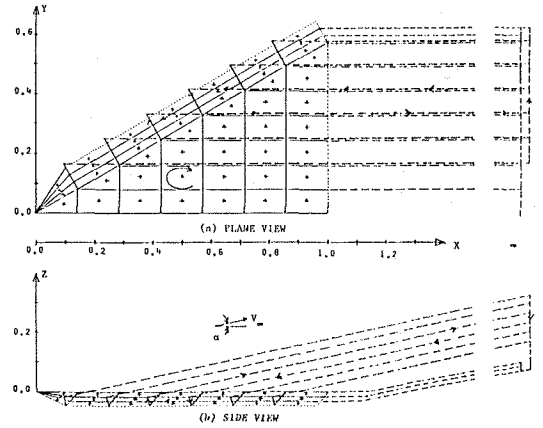

Fig. 12. Vortex loop panel arrangement and initial guess for free vortices (NW=7, NF=3).

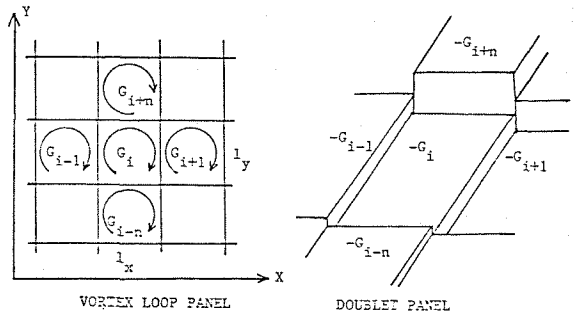

Fig. 13. Notation for velocity jump formula.

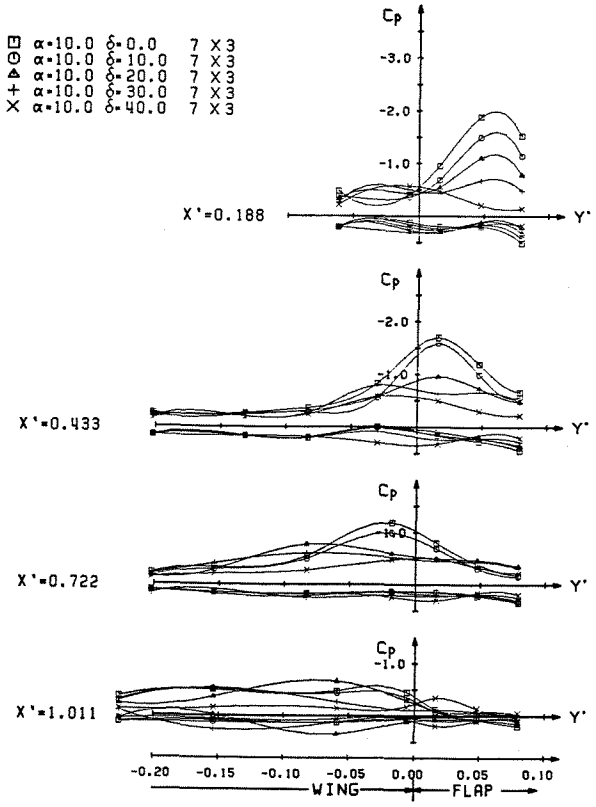

Fig. 14. Effect of flap deflection at $\alpha=10°$ (computed).

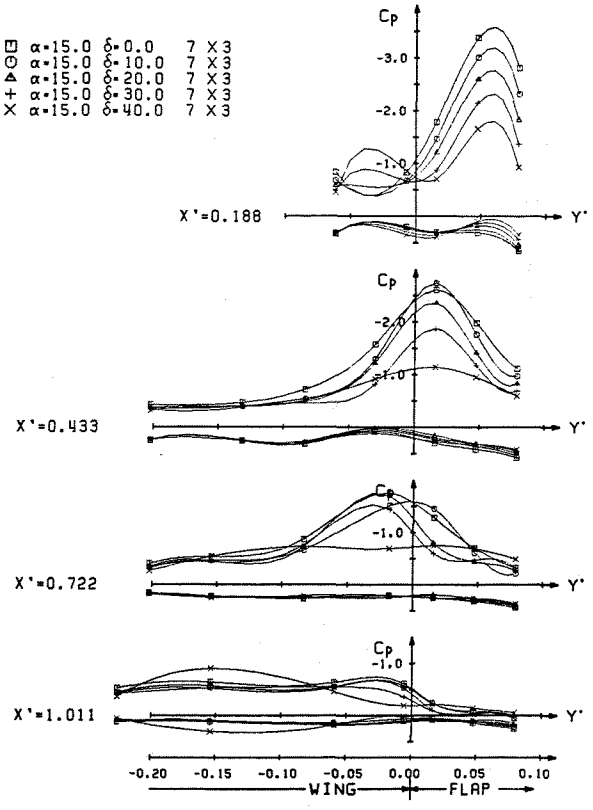

Fig. 15. Effect of flap deflection at $\alpha=15°$ (computed).

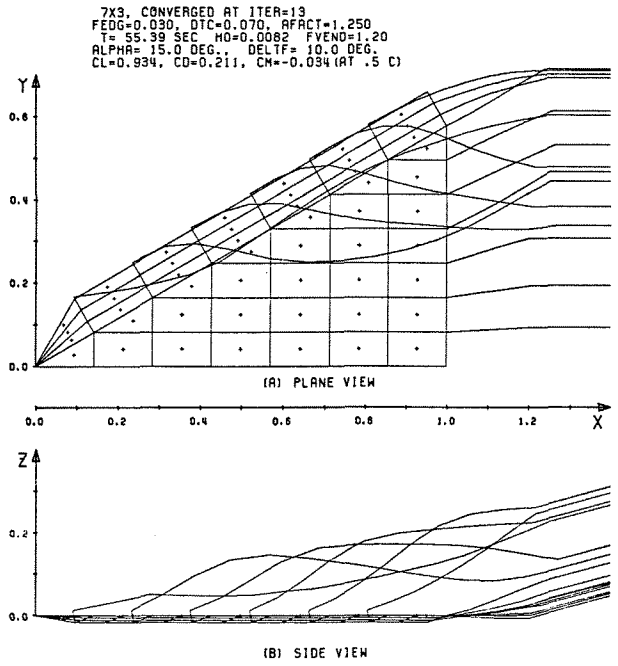

Fig. 16. Converged shape of free vortices at $\alpha=15°$, $\delta=10°$

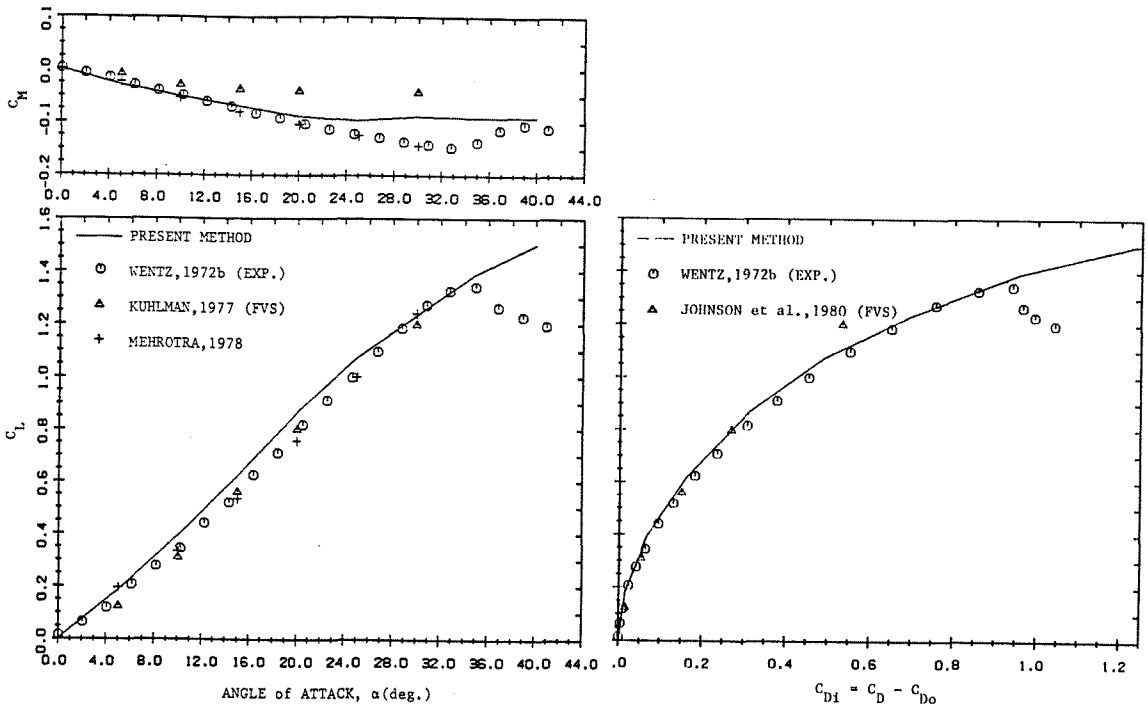

Fig. 17. Comparison of longitudinal aerodynamic load characteristics for a 74° delta wing.